



Investigation on grinding force and machining quality during rotary ultrasonic grinding deep-small hole of fluorophlogopite ceramics

Guojun Dong¹ · Liming Zhang¹

Received: 8 March 2019 / Accepted: 9 July 2019 / Published online: 26 July 2019
© Springer-Verlag London Ltd., part of Springer Nature 2019

Abstract

Fluorophlogopite ceramics is widely used in the fields of aerospace and biomedicine, and the machining of deep-small hole for fluorophlogopite ceramics is a focus in the field of precision and ultra-precision machining. In this work, the trajectory and brittle-to-ductile transition depth of single abrasive during rotary ultrasonic grinding process were analyzed. The rotary ultrasonic grinding and common grinding tests of deep-small holes for fluorophlogopite ceramics were performed on an ultrasonic vibration and precision machining center. The axial grinding force was obtained by wavelet denoising, the roundness deviation was calculated by using Canny and gray level detection methods, and the internal surface roughness was measured by using laser scanning confocal microscopy. The experimental results indicated that compared with the common grinding, rotary ultrasonic grinding could effectively decrease the grinding force, roundness deviation, and the value of surface roughness. In addition, the grinding force, roundness deviation, and the value of surface roughness decreased as the spindle speed and ultrasonic power increased, and they increased as the feed speed increased. This work was of significance for realizing the high efficiency and precision machining of deep-small holes of the hard-brittle materials.

Keywords Fluorophlogopite ceramics · Rotary ultrasonic grinding · Deep-small hole · Roundness deviation · Internal surface roughness

Nomenclature

A	Ultrasonic amplitude	K_{IC}	Fracture toughness of workpiece
a	Half of the length of abrasive diagonal	H	Vickers hardness of workpiece
f	Ultrasonic frequency	P^*	Critical load of crack generation
n	Spindle speed	P	Indentation load
r	Distance from the abrasive centroid to wheel center	α	Dimensionless constant which is related to abrasive geometry
θ_1	Initial phase	δ	Cutting depth related to tool amplitude
Z_1	Ultrasonic vibration along the axis direction	θ	Half of the angle between the edge of the abrasive
θ_2	Initial phase of ultrasonic vibration along the axis direction	h_m^*	Critical machining depth of single grain under the static load
v_f	Feed speed	m	Weight of single abrasive
v_x	Grinding speed of single abrasive in X direction	K_{IC}^d	Dynamic fracture toughness
v_y	Grinding speed of single abrasive in Y direction	λ_0	Dimensionless constant which is related to abrasive geometry
v_z	Grinding speed of single abrasive in Z direction		
h_{md}^*	Brittle-to-ductile transition depth during ultrasonic grinding		

✉ Guojun Dong
dongguojun@hit.edu.cn

¹ School of Mechatronics Engineering, Harbin Institute of Technology, Harbin 150001, China

1 Introduction

With the development of the cutting-edge technologies in the fields of optics, electronics, medicine, biotechnology, aerospace and so on, engineering ceramics, such as fluorophlogopite ceramics [1], SiC ceramics [2], and Lu₂O₃

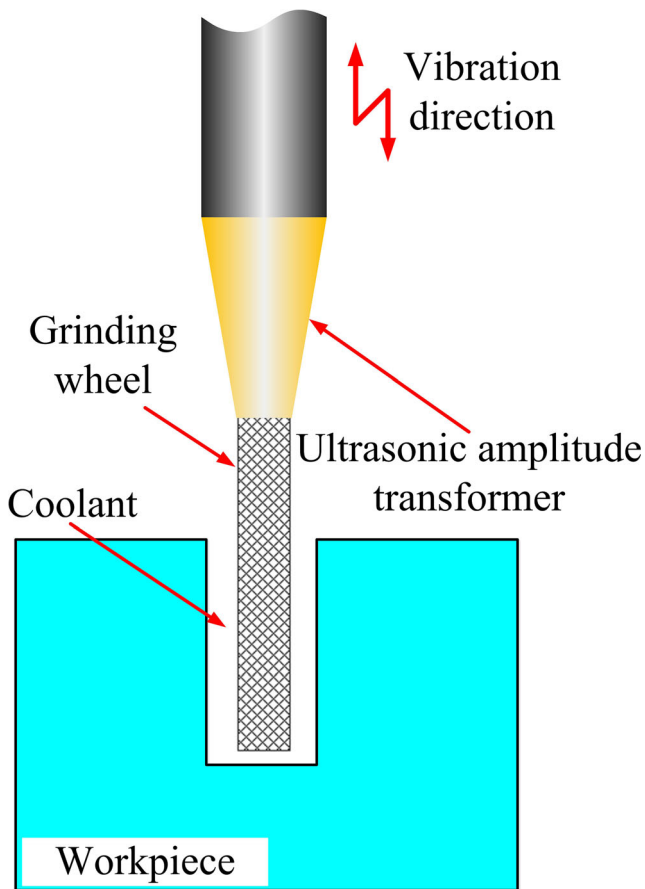


Fig. 1 Diagrammatic sketch of ultrasonic grinding small-deep holes

ceramics [3], have become the focus of advanced manufacturing and processing due to their high strength, high hardness, low coefficient of thermal expansion, and steady chemical properties. However, as typical hard-brittle materials, these materials are difficult to machine due to their high hardness and low fracture toughness, which has become a bottleneck problem in the popularization and application of engineering ceramics [4–6]. Micro-machining technology is widely used in the fields of optics, electronics, medicine, biotechnology, aerospace, and so on [7–9]. Most of the micro-machining methods for engineering ceramics are hole-machining which

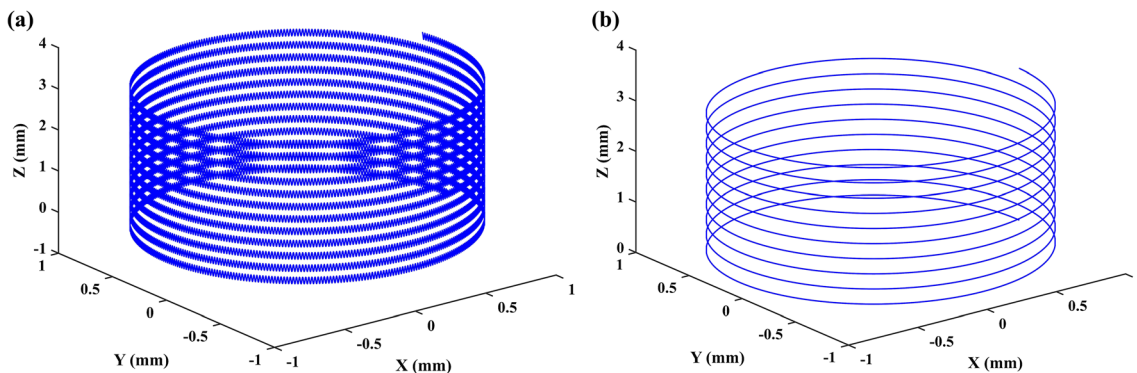


Fig. 2 Trajectories of single abrasive under a rotary ultrasonic grinding and b common grinding

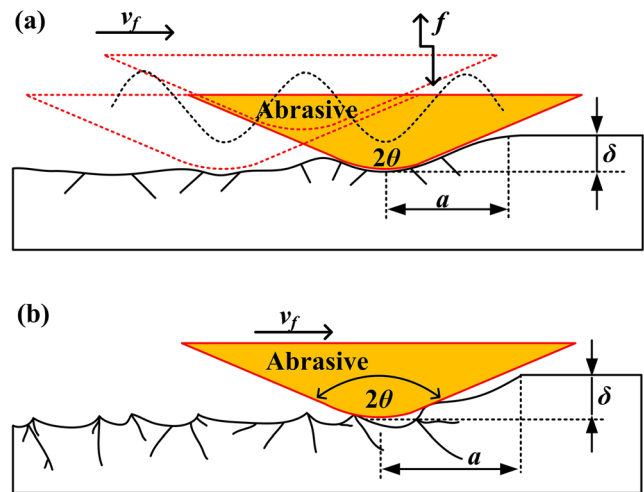


Fig. 3 Diagram of interaction between diamond abrasive and workpiece under a rotary ultrasonic grinding and b common grinding

accounts for about 40% of the total processing of engineering ceramics [10]. At present, common drilling technology is the most widely used in the fields of micro-hole processing. However, the deflection and poor centering of micro-bits, poor chip removal, difficult heat dissipation, edge broken occur easily during the common drilling process of hard-brittle materials [11]. Especially for deep-small holes with a ratio of length to diameter above 10, common drilling technology is difficult to satisfy the accuracy requirements [12].

In order to improve the machining efficiency and surface integrity of hard-brittle materials, considerable non-traditional processing methods assisted by high-energy beam have been proposed, such as laser assistant machining [13, 14], ion beam assistant machining [15], electron beam assistant machining [16], and plasma assistant machining [17]. Compared with the high-energy beam-assisted machining, rotary ultrasonic grinding for the machining of deep-small hole has many advantages, such as no thermal damage, low residual stress, and no deterioration layer on the machined surface/subsurface. Moreover, the machining processing of rotary ultrasonic grinding does not depend on the electrical conductivity and chemical properties of the workpiece. Compared with traditional drilling, rotary

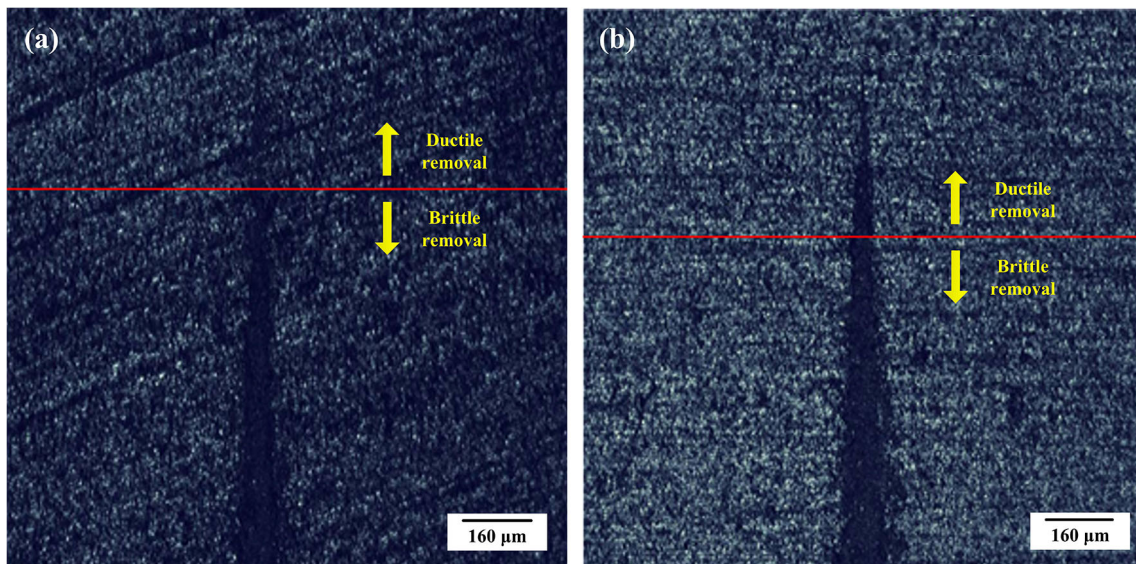


Fig. 4 Surface morphologies generated by a common scratching and b ultrasonic-assisted scratching

ultrasonic grinding can achieve larger length-diameter ratio, reduce cutting force, and improve tool durability, machining efficiency, and surface integrity [18–20]. Wang et al. [21] performed the rotary ultrasonic drilling experiments of K9 glass and single crystal sapphire; the experimental results indicated that brittle removal is the main removal form during the machining process. A theoretical model for predicting the size of edge chipping was developed and verified by the experimental data. The model indicated that increasing the ultrasonic amplitude and spindle speed could effectively reduce the size of edge chipping. Wei et al. [22] carried out the rotary ultrasonic grinding

experiments of engineering ceramics and proposed a new evaluation index which could better evaluate the surface roughness of the machined surface. The evaluation model was verified by the rotary ultrasonic grinding experiments. Lv et al. [23] compared the differences of surface morphology and subsurface damage between common and rotary ultrasonic grinding, and the experimental results demonstrated that the values of surface roughness and subsurface damage depth in rotary ultrasonic grinding were lower than that in common grinding, and increasing grinding speed and decreasing grinding depth and feed speed could improve the surface quality and reduce the subsurface damage

Fig. 5 Experimental device of ultrasonic grinding small-deep holes. a and b Experimental device. c and d Grinding wheels

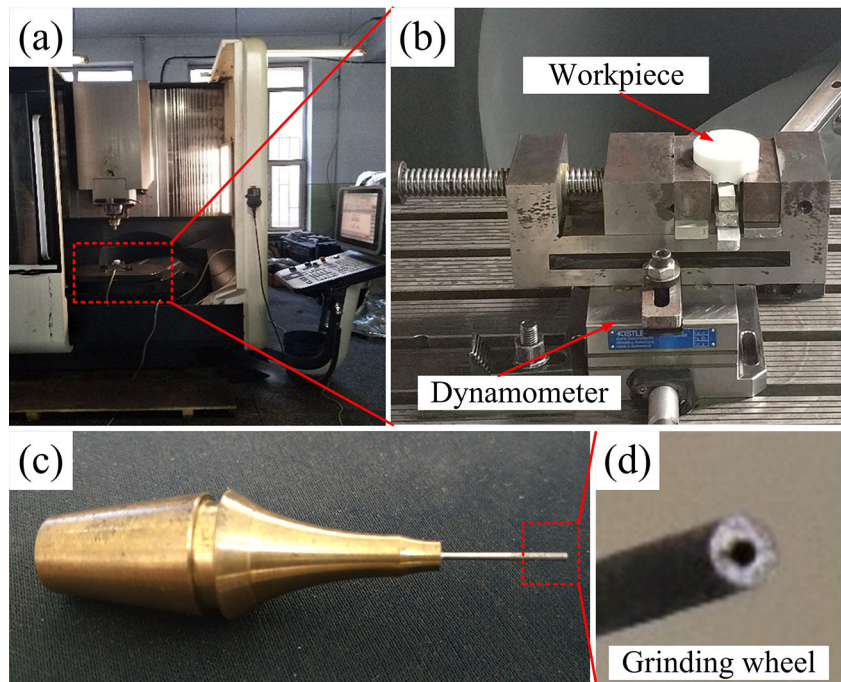


Table 1 Constituent components of fluorophlogopite ceramics (%)

Specification	SiO ₂	MgO	Al ₂ O ₃	K ₂ O	B ₂ O ₃	F
Content	46	17	16	10	7	4

depth. Feng et al. [24] investigated the tearing defects of C/SiC composites induced by the rotary ultrasonic machining, and found that compared with the common drilling, rotary ultrasonic drilling could reduce the tearing defect at the hole exit more than 60%. In addition, the tearing defects could be further reduced by increasing the spindle speed and ultrasonic amplitude or decreasing the feed rate.

In this work, the theoretical trajectory and brittle-to-ductile transition depth of single grain during rotary ultrasonic grinding process were analyzed, and rotary ultrasonic grinding experiments for deep-small holes of fluorophlogopite ceramics were systematically performed. The roundness deviation, internal surface roughness of deep-small holes, and grinding force of rotary ultrasonic grinding were analyzed. This work was of great significance for the high-efficiency and precision machining of fluorophlogopite ceramics.

2 Theoretical trajectory analysis and brittle-to-ductile transition depth of single abrasive during rotary ultrasonic grinding process

The diagrammatic sketch of ultrasonic grinding small-deep holes is shown in Fig. 1, and it can be found that the vibration direction produced by piezoelectric ceramics was along the axis direction.

The theoretical trajectory of single abrasive plays an important role on analyzing the grinding force and material removal efficiency during the rotary ultrasonic grinding process. As presented in Eq. (1), in addition to the circumferential motion around the spindle and the linear feed motion along the axis direction, the abrasives vibrate periodically along the axis direction.

$$\begin{cases} X = r \cos\left(\frac{n\pi t}{30} + \theta_1\right) \\ Y = r \sin\left(\frac{n\pi t}{30} + \theta_1\right) \\ Z = Z_1 + v_f t \\ Z_1 = A \sin(2\pi f t + \theta_2) \end{cases} \quad (1)$$

Table 2 Mechanical properties of fluorophlogopite ceramics

Specification	Density	Young's modulus	Poisson ratio	Shear modulus	Compression strength	Fracture toughness	Bending strength	Hardness
Unit	g/cm ³	GPa	–	Gpa	MPa	MPa·m ^{0.5}	MPa	GPa
Value	2.52	66.9	0.29	25.5	34.5	1.58	108	2.54

Table 3 Grinding conditions for single-factor tests

Group no.	Grinding parameters		
	n_s (rpm)	v_f (mm/min)	P (%)
1~5	2000~10,000	3	0
6~9	6000	1.8~4.2	0
10~14	2000~10,000	3	100
15~18	6000	1.8~4.2	100
19~22	6000	3	20~80

where r is the distance from the abrasive centroid to wheel center, n is spindle speed, θ_1 is the initial phase, Z_1 is the ultrasonic vibration along the axis direction, and θ_2 is the initial phase of ultrasonic vibration along the axis direction.

When Z_1 is equal to 0, Eq. (1) is the trajectory equation of common grinding. The trajectories of single abrasive under rotary ultrasonic grinding and common grinding are presented in Fig. 2.

As presented in Eq. (2), the grinding speeds of single abrasive in the three direction under rotary ultrasonic grinding can be acquired according to Eq. (1).

$$\begin{cases} v_x = -\frac{n\pi r}{30} \sin\left(\frac{n\pi t}{30} + \theta_1\right) \\ v_y = \frac{n\pi r}{30} \cos\left(\frac{n\pi t}{30} + \theta_1\right) \\ v_z = v_f \end{cases} \quad (2)$$

To simplify the modeling, the following assumptions were made: (a) All the abrasives are evenly distributed on the surface of the grinding wheel. (b) All abrasive grains have the same size. (c) The frequency and amplitude are stable during the grinding process. The mass of a single abrasive was used to calculate the impact force on the abrasive [2, 21].

When there is no ultrasonic vibration on the grinding wheel, the diamond abrasives on the wheel face will contact the material surface under static load. Because the actual diamond particles are irregular in shape, the diamond abrasives are simplified as Vickers hardness indenter, as shown in Fig. 3.

The critical load of crack generation in indentation fracture mechanics can be expressed as Eq. (3).

$$P^* = \lambda_0 \left(\frac{K_{IC}}{H}\right)^3 K_{IC} \quad (3)$$



Fig. 6 Machined workpiece cut by a cutting machine

where λ_0 is a dimensionless constant which is related to abrasive geometry, and it is 2.2×10^3 for Vickers indenter. K_{IC} is the fracture toughness of fluorophlogopite ceramics, and H is Vickers hardness of fluorophlogopite ceramics.

In plastic regime, indentation load and indentation depth can be expressed using Eq. (4).

$$P = \alpha\pi a^2 H \tag{4}$$

where α is a dimensionless constant which is related to abrasive geometry, δ is the cutting depth which is related to the tool amplitude, and θ is half of the angle between the edge of the abrasive. a is half of the length of abrasive diagonal, and it can be calculated by Eq. (5).

$$a = \delta \times \tan \theta \tag{5}$$

As presented in Eq. (6), the critical machining depth of single grain under the static load could be calculated according to Eqs. (3)–(5).

$$h_m^* = \left(\frac{\lambda_0}{\alpha\pi}\right)^{0.5} \left(\frac{K_{IC}}{H}\right)^2 \frac{1}{\tan\theta} \tag{6}$$

When the diamond wheel was subjected to ultrasonic vibration, the abrasives on the end-face of the wheel were subjected to high-frequency vibration. Due to the ultrasonic vibration action, the abrasives have a certain acceleration, thus forming impact load. When the sum of indentation load and impact load was less than the critical load, cracks would not

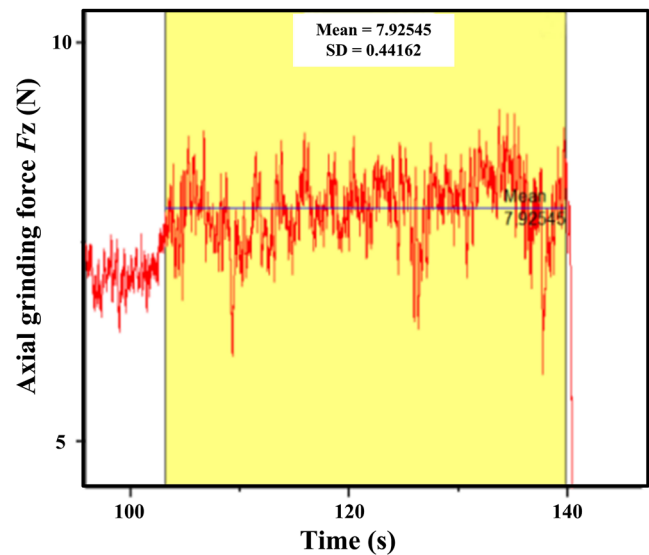


Fig. 8 Dynamic signals of axial grinding force ($n_s = 10,000$ rpm, $v_f = 30$ mm/min, $P = 100\%$)

occur, and the ductile rotary ultrasonic grinding of ceramic materials could be realized, as shown in Eq. (7).

$$P + m \cdot (-Aw^2 \cos(wt)) \leq P^* \tag{7}$$

where m is the weight of single abrasive.

Therefore, the brittle-to-ductile transition depth during ultrasonic grinding can be respected by Eq. (8). When $h \leq h_{md}^*$, the ductile grinding of fluorophlogopite ceramics could be realized.

$$h_{md}^* = \left(\frac{\lambda_0}{\alpha\pi}\right)^{0.5} \left(\frac{K_{IC}^d}{H}\right)^2 \frac{1}{\tan\theta} + \left(\frac{Am\cos wt}{\alpha\pi H}\right)^{0.5} \frac{w}{\tan\theta} \tag{8}$$

where K_{IC}^d is dynamic fracture toughness of fluorophlogopite ceramics, which is determined by Eq. (9).

$$K_{IC}^d = 0.6875K_{IC} \tag{9}$$

According to Eqs. (6) and (8), the brittle-to-ductile transition depths of single abrasive under common scratching and ultrasonic-assisted scratching ($f = 25$ KHz, $A = 7$ μ m) were calculated as 0.740 and 1.114 μ m, respectively. In addition, common scratching and ultrasonic-assisted scratching tests were also performed to verify the theoretical model. As shown in Fig. 4, the brittle-to-ductile transition depths were measured by using laser confocal microscopy (OLS3000), and the experimental results indicated that the brittle-to-ductile transition

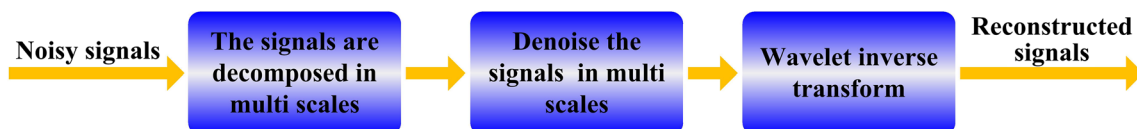


Fig. 7 Flow chart of the wavelet denoising

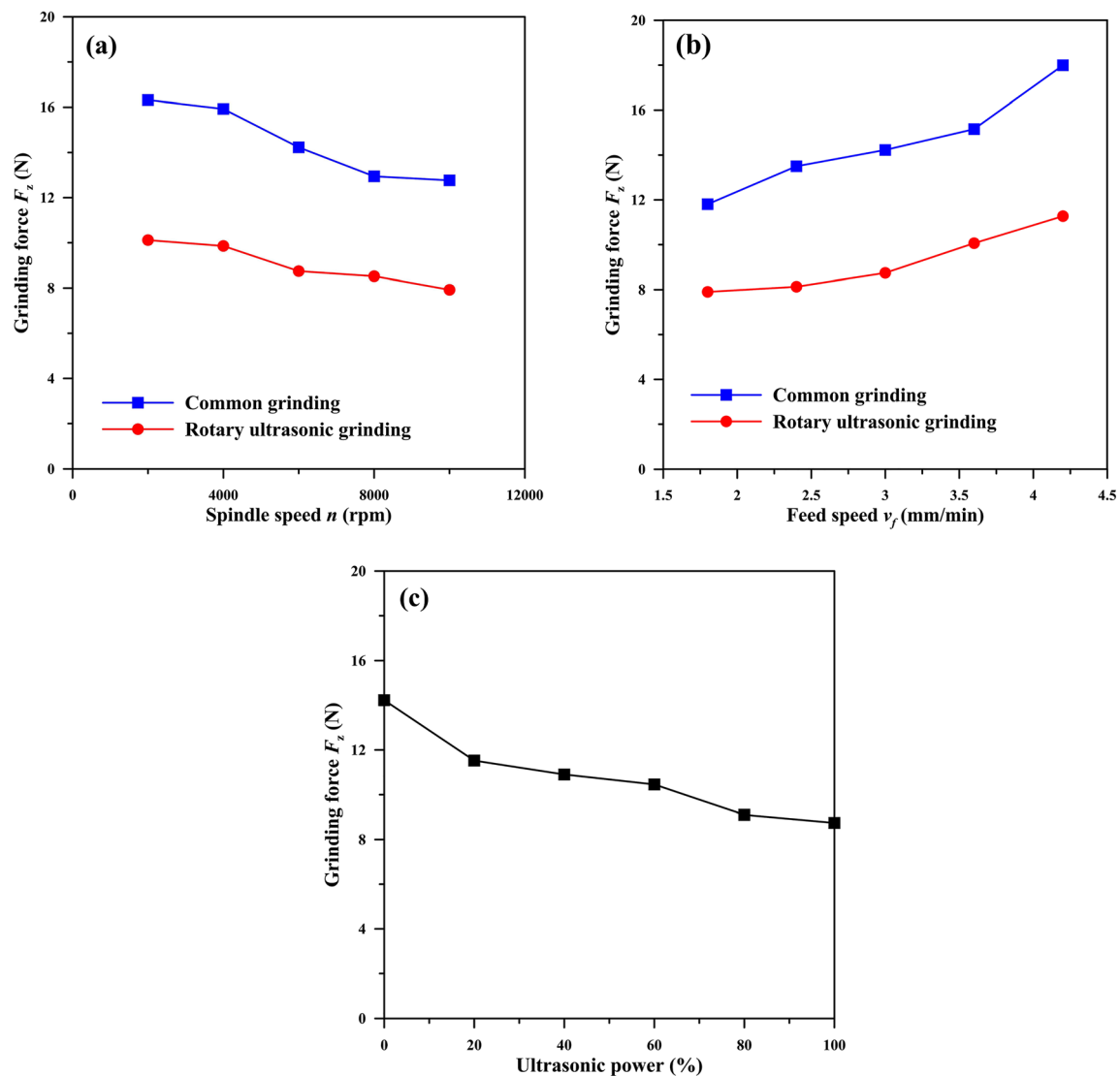


Fig. 9 Influence of grinding parameters on axial grinding force. **a** Spindle speed vs axial grinding force. **b** Feed speed vs axial grinding force. **c** Ultrasonic power vs axial grinding force

depths of single abrasive under common scratching and ultrasonic-assisted scratching ($f = 25\text{KHz}$, $A = 7\ \mu\text{m}$) were 0.698 and 1.203 μm , respectively. The theoretical and experimental results were in good agreement. Both theoretical and experimental results demonstrated that the ultrasonic vibration could effectively improve the brittle-to-ductile transition depth of hard-brittle materials.

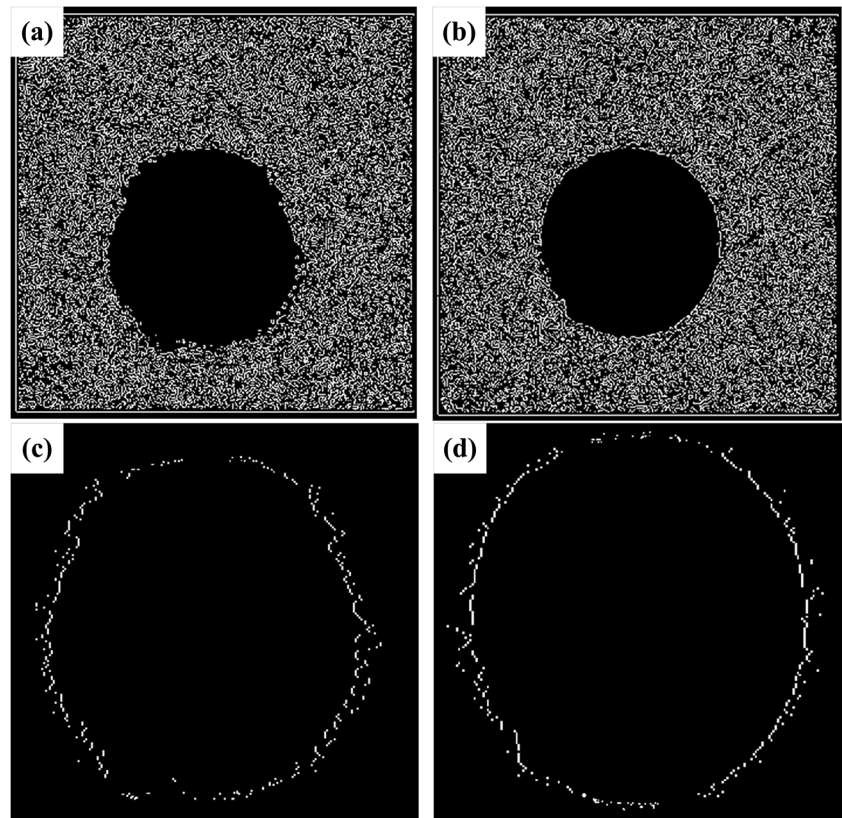
3 Experimental device and conditions

As shown in Fig. 5a, the rotary ultrasonic grinding experiment of deep-small holes for fluorophlogopite ceramics was performed on an ultrasonic vibration and precision machining center, DMG Ultrasonic 70-5 Linear. As presented in Fig. 5b, the grinding force was measured by a quartz three-component dynamometer, Kistler 9257B.

Electroplated diamond wheel (D64) was used in the grinding experiment, as shown in Fig. 5 c and d. The diameter and length of the grinding wheel were 1 and 15 mm, respectively. The frequency of ultrasonic machining is 30305 Hz, and the maximum output power is 300 W. High-performance synergy coolant of Blaso was used during the grinding process. The workpiece was fluorophlogopite ceramics, and the workpiece size was $\Phi 45\text{mm} \times 12\ \text{mm}$. The constituent components and mechanical properties of fluorophlogopite ceramics are shown in Tables 1 and 2, respectively. The diameter and depth of small-depth holes were 1.2 mm and 7 mm, respectively. The ratio of depth to diameter is approximately 5.83.

The single-factor test was designed to research the influences of grinding parameters on axial grinding force, roundness deviation, and internal surface roughness, as shown in Table 3.

Fig. 10 **a** Edge profile of common grinding using Canny detection method. **b** Edge profile of rotary ultrasonic grinding using Canny detection method. **c** Edge profile of common grinding using detection method of gray level. **d** Edge profile of rotary ultrasonic grinding using detection method of gray level



After the grinding experiments of fluorophlogopite ceramics, the workpiece was cleaned by absolute ethyl alcohol. The roundness deviation and internal surface roughness were measured by a laser confocal microscope (OLS3000). In order to measure the internal surface roughness, the machined workpiece was cross sectioned by a cutting machine, as shown in Fig. 6.

4 Results and discussions

4.1 Influence of grinding parameters on axial grinding force

Because the noise produced by the machine tool can affect the detection and processing of the data of grinding force, the data acquired by the dynamometer should be processed by wavelet denoising. The flow chart of the wavelet denoising is presented in Fig. 7.

Because the grinding forces in *X*-axis direction and *Y*-axis direction were very small in the grinding process of deep holes, the grinding force in *Z*-axis direction was studied in this work. The Savitzky-Golay method of wavelet denoising was chosen in this work. The filtering window is 200. Because the grinding force increases with the increase of grinding depth, the maximum grinding force was chosen as the object. After noise reduction

and reconstruction processes, the average value of the maximum grinding force was measured as about 7.925 N and the standard deviation was measured as about 0.442 N, as shown in Fig. 8.

The influences of grinding parameters on grinding force during rotary ultrasonic grinding and common grinding deep-small holes of fluorophlogopite ceramics are presented in Fig. 9. It can be found that under the same grinding parameters, the axial grinding force produced by common grinding was much greater than that produced by rotary ultrasonic grinding. This occurred because the rotary ultrasonic vibration of abrasives was beneficial to reduce the friction between the diamond tool and workpiece. In addition, the grinding chips under ultrasonic vibration were more conducive to be removed by the grinding coolant. Therefore, the grinding heat during ultrasonic vibration grinding was effectively reduced, which resulted in the decrease of grinding force. With the increase of spindle speed and ultrasonic power, the axial grinding force decreased, while it increased as the feed speed increased. This occurred because increasing the spindle speed could effectively reduce the maximum undeformed chip thickness, which resulted in the decrease of axial grinding force. The increase of feed speed increased the material removal rate and the maximum cutting depth of diamond abrasives, which resulted in the increase of axial grinding force. Although

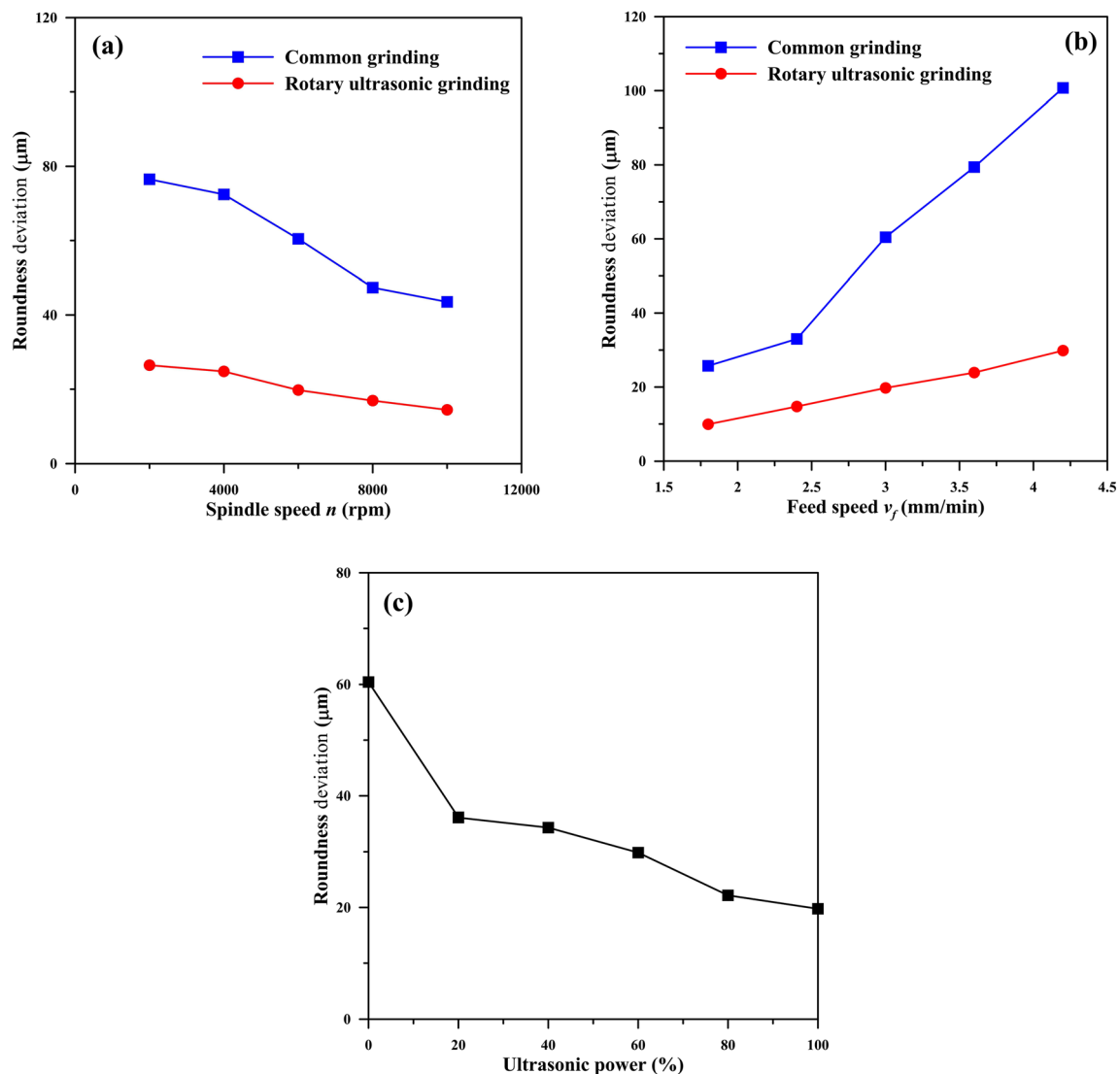


Fig. 11 Influence of grinding parameters on roundness deviation of deep-small holes. **a** Spindle speed vs roundness deviation. **b** Feed speed roundness deviation. **c** Ultrasonic power roundness deviation

increasing the feed speed could improve the machining efficiency, it could deteriorate the surface quality of the deep-small holes and shorten the service life of grinding wheels. In addition, it was difficult to machine the deep-small holes at a high feed speed under the common grinding because the grinding wheel was easily broken under the common grinding. Therefore, when the feed was high, rotary ultrasonic grinding can ensure the machining efficiency, effectively reduce the axial grinding force and improve the service life of grinding wheels. When the ultrasonic power increased, the effective contact time between the abrasives and workpiece decreased. As the ultrasonic frequency of the machine tool was constant, increasing the ultrasonic power could increase the corresponding ultrasonic amplitude and decrease the axial grinding force.

4.2 Influence of grinding parameters on roundness deviation of deep-small hole

Roundness deviation is one of the important indicators to evaluate the processing quality of deep-small holes. In this work, the roundness deviation was measured by using digital image processing technology. Firstly, the ground hole was observed by using a laser confocal microscope, and the images of hole morphology were directed out. Then, the images were processed by median filter with the software of MATLAB, which could separate the workpiece and get the corresponding binary graph. Finding the edge profile of the holes by Canny detection method can obviously improve the progress of edge detection, effectively reduce the impact of the noise, and achieve a high-precision boundary detection. For this method, the strong and weak boundaries were

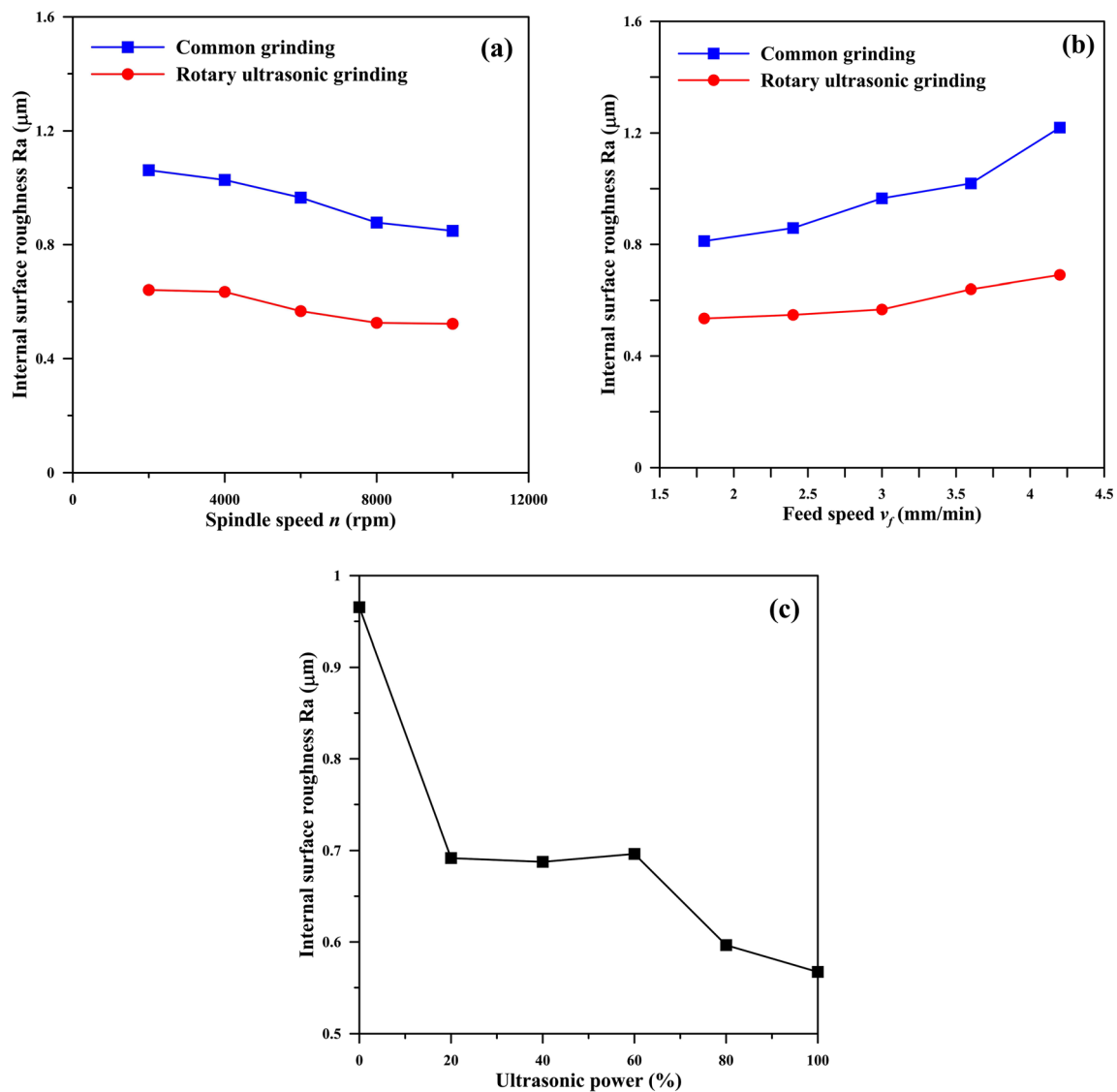


Fig. 12 Influence of grinding parameters on internal surface roughness. **a** Spindle speed vs internal surface roughness. **b** Feed speed vs internal surface roughness. **c** Ultrasonic power vs internal surface roughness

distinguished by setting two thresholds. If the two kinds of boundaries were connected, the weak boundaries would be output, as shown in Fig. 10a and b. Then scan the image center upward to left, upward to right, downward to left, and downward to right row by row to find the edge points, and extract the edges of deep holes by this method, as shown in Fig. 10c and d. Finally, the roundness deviation was calculated by MATLAB. From Fig. 10, it could be found that the edge profile machined by rotary ultrasonic grinding was better than that machined by common grinding.

The relationship between grinding parameters with roundness deviation of deep-small holes is presented in Fig. 11, which indicates that the roundness deviation of deep-small holes decreased as the spindle speed and ultrasonic power increased, and increased as the feed speed increased both in common grinding and rotary ultrasonic grinding process. This

occurred because a higher grinding speed and ultrasonic power could lead to the decreasing of the grinding force, which effectively decreased the stress of the hole edge and the roundness deviation. Because a higher feed speed resulted in a larger grinding force, which lead to a large-area edge broken during the machining process of ceramic materials, therefore, the roundness deviation increased as the feed speed increased.

4.3 Influence of grinding parameters on internal surface roughness

The influence of grinding parameters on internal surface roughness and the surface morphologies under different grinding parameters are presented in Figs. 12 and 13, respectively. It can be found that rotary ultrasonic grinding could effectively decrease the value of internal surface roughness compared

with the common grinding. In addition, increasing the spindle speed and ultrasonic power could decrease the value of internal surface roughness, while increasing the feed speed could increase the value of internal surface roughness. This occurred because the ultrasonic vibration effectively removed the ladder-shaped striations caused by the spiral trajectory of the grinding wheel, which could decrease the value of the internal surface roughness, as shown in Fig. 13a and b. When the feed speed increased, the interaction between abrasives decreased and the maximum undistorted chip thickness increased, which resulted in more residual materials and higher roughness, as shown in Fig. 13b and c. Increasing the spindle speed could reduce the maximum deformed chip thickness and the residual height of grinding trajectory, which resulted in the reduction of the value of the surface roughness.

5 Conclusions

The rotary ultrasonic grinding and common grinding tests of deep-small hole for fluorophlogopite ceramics were performed on an ultrasonic vibration and precision machining center, and the grinding force, roundness deviation, and the value of surface roughness were systematically studied in this

work. The major conclusions from this study are summarized as follows:

- (1) The trajectory and brittle-to-ductile transition depth of single abrasive during rotary ultrasonic grinding process were analyzed. Both theoretical and experimental results demonstrated that the ultrasonic vibration could effectively improve the brittle-to-ductile transition depth of hard-brittle materials.
- (2) Compared with the common grinding, rotary ultrasonic grinding could effectively decrease the grinding force, roundness deviation, and the value of surface roughness, which indicated that rotary ultrasonic grinding is an effective means to machine deep-small holes of hard-brittle materials.
- (3) The influences of the grinding parameters on the grinding force, roundness deviation, and value of surface roughness were analyzed in this work. The experimental results indicated that the grinding force, roundness deviation, and value of surface roughness decreased as spindle speed and ultrasonic power increased, and they increased as feed speed increased. Therefore, under the premise of guaranteeing processing efficiency, increasing the spindle speed and ultrasonic power and decreasing the feed speed

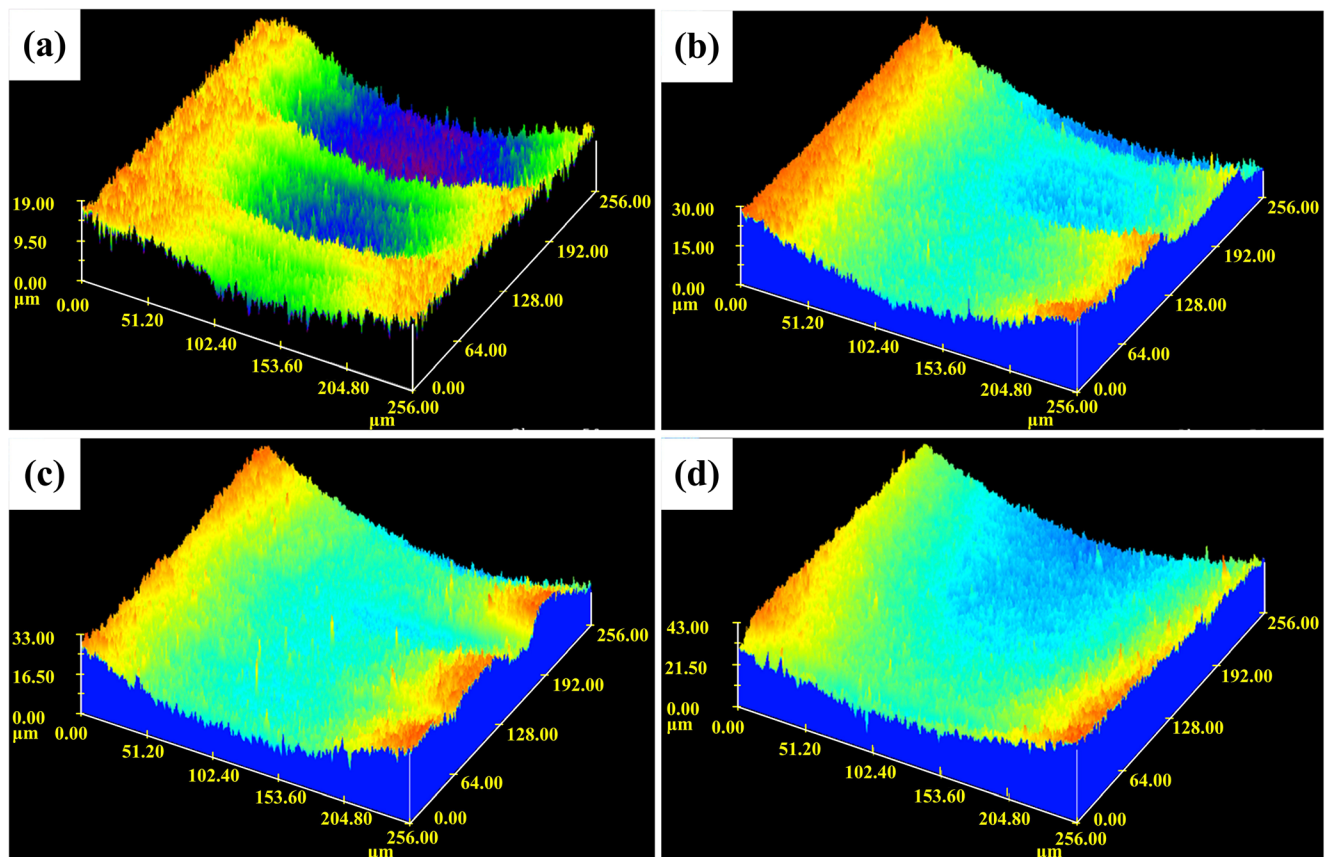


Fig. 13 Surface morphologies under different grinding parameters. **a** $n_s = 6000$ rpm, $v_f = 30$ mm/min, and $P = 0$. **b** $n_s = 6000$ rpm, $v_f = 30$ mm/min, and $P = 100\%$. **c** $n_s = 6000$ rpm, $v_f = 18$ mm/min, and $P = 100\%$. **d** $n_s = 10,000$ rpm, $v_f = 30$ mm/min, and $P = 100\%$

can effectively improve machining quality of the deep-small hole of fluorophlogopite ceramics.

Funding information This work was supported by the National Natural Science Foundation of China (Grant No. 51675131).

References

- Ma L, Li C, Chen J, Li W, Tan Y, Wang C, Zhou Y (2017) Prediction model and simulation of cutting force in turning hard-brittle materials. *Int J Adv Manuf Technol* 91(1-4):165–174
- Li C, Zhang F, Meng B, Liu L, Rao X (2017) Material removal mechanism and grinding force modelling of ultrasonic vibration assisted grinding for SiC ceramics. *Ceram Int* 43(3):2981–2993
- Li C, Zhang F, Wang X, Rao X (2018) Repeated nanoscratch and double nanoscratch tests of Lu₂O₃ transparent ceramics: material removal and deformation mechanism, and theoretical model of penetration depth. *J Eur Ceram Soc* 38(2):705–718
- Ma L, Gong Y, Chen X (2014) Study on surface roughness model and surface forming mechanism of ceramics in quick point grinding. *Int J Mach Tools Manuf* 77:82–92
- Li C, Li X, Wu Y, Zhang F, Huang H (2019) Deformation mechanism and force modelling of the grinding of YAG single crystals. *Int J Mach Tools Manuf* 143:23–37
- Li C, Zhang F, Ma Z, Ding Y (2017) Modeling and experiment of surface error for large-aperture aspheric SiC mirror based on residual height and wheel wear. *Int J Adv Manuf Technol* 91(1-4):13–24
- Gao S, Huang H (2017) Recent advances in micro-and nano-machining technologies. *Front Mech Eng* 12(1):18–32
- Crichton ML, Archer-Jones C, Meliga S, Edwards G, Martin D, Huang H, Kendall MA (2016) Characterising the material properties at the interface between skin and a skin vaccination microprojection device. *Acta Biomater* 36:186–194
- Suganthi XH, Natarajan U, Ramasubbu N (2015) A review of accuracy enhancement in microdrilling operations. *Int J Adv Manuf Technol* 81(1-4):199–217
- Hamade RF, Ismail F (2005) A case for aggressive drilling of aluminum. *J Mater Process Technol* 166(1):86–97
- Song X, Lieh J, Yen D (2007) Application of small-hole dry drilling in bimetal part. *J Mater Process Technol* 186(1-3):304–310
- Ni H, Gong H, Dong YH, Fang FZ, Wang Y (2018) A comparative investigation on hybrid EDM for drilling small deep holes. *Int J Adv Manuf Technol* 95(1-4):1465–1472
- Yang B, Shen X, Lei S (2009) Mechanisms of edge chipping in laser-assisted milling of silicon nitride ceramics. *Int J Mach Tools Manuf* 49(3-4):344–350
- Guerrini G, Lutey AH, Melkote SN, Fortunato A (2018) High throughput hybrid laser assisted machining of sintered reaction bonded silicon nitride. *J Mater Process Technol* 252:628–635
- Volkert CA, Busch S, Heiland B, Dehm G (2004) Transmission electron microscopy of fluorapatite–gelatine composite particles prepared using focused ion beam milling. *J Microsc* 214(3):208–212
- Spinney PS, Howitt DG, Smith RL, Collins SD (2010) Nanopore formation by low-energy focused electron beam machining. *Nanotechnology* 21(37):375301
- Deng H, Endo K, Yamamura K (2017) Damage-free finishing of CVD-SiC by a combination of dry plasma etching and plasma-assisted polishing. *Int J Mach Tools Manuf* 115:38–46
- Egashira K, Kumagai R, Okina R, Yamaguchi K, Ota M (2014) Drilling of microholes down to 10 μm in diameter using ultrasonic grinding. *Precis Eng* 38(3):605–610
- Bertsche E, Ehmann K, Malukhin K (2013) An analytical model of rotary ultrasonic milling. *Int J Adv Manuf Technol* 65(9-12):1705–1720
- Li ZC, Jiao Y, Deines TW, Pei ZJ, Treadwell C (2005) Rotary ultrasonic machining of ceramic matrix composites: feasibility study and designed experiments. *Int J Mach Tools Manuf* 45(12-13):1402–1411
- Wang J, Feng P, Zhang J, Zhang C, Pei Z (2016) Modeling the dependency of edge chipping size on the material properties and cutting force for rotary ultrasonic drilling of brittle materials. *Int J Mach Tools Manuf* 101:18–27
- Wei S, Zhao H, Jing J (2015) Investigation on three-dimensional surface roughness evaluation of engineering ceramic for rotary ultrasonic grinding machining. *Appl Surf Sci* 357:139–146
- Lv D, Wang H, Zhang W, Yin Z (2016) Subsurface damage depth and distribution in rotary ultrasonic machining and conventional grinding of glass BK7. *Int J Adv Manuf Technol* 86(9-12):2361–2371
- Feng P, Wang J, Zhang J, Zheng J (2017) Drilling induced tearing defects in rotary ultrasonic machining of C/SiC composites. *Ceram Int* 43(1):791–799

Publisher's note Springer Nature remains neutral with regard to jurisdictional claims in published maps and institutional affiliations.